

Exploitation of Electromagnetic Models for Sea Wind Speed Estimation from C-Band Sentinel-1 Images

Tran Vu La¹, Ali Khenchaf¹, Fabrice Comblet¹, Carole Nahum², Helmi Ghanmi¹

¹Lab-STICC, UMR CNRS 6285, ENSTA Bretagne, Brest, France

²French General Directorate for Armament (DGA), Paris, France

Email: tran_vu.la@ensta-bretagne.fr, Ali.Khenchaf@ensta-bretagne.fr,
Fabrice.Comblet@ensta-bretagne.fr, carole.nahum@intradef.gouv.fr

Received 26 January 2016; accepted 26 March 2016; published 30 March 2016

Copyright © 2016 by authors and Scientific Research Publishing Inc.

This work is licensed under the Creative Commons Attribution International License (CC BY).

<http://creativecommons.org/licenses/by/4.0/>



Open Access

Abstract

Among the different available wind sources, *i.e. in situ* measurements, numeric weather models, the retrieval of wind speed from Synthetic Aperture Radar (SAR) data is one of the most widely used methods, since it can give high wind resolution cells. For this purpose, one can find two principal approaches: via electromagnetic (EM) models and empirical (EP) models. In both approaches, the Geophysical Model Functions (GMFs) are used to describe the relation of radar scattering, wind speed, and the geometry of observations. By knowing radar scattering and geometric parameters, it is possible to invert the GMFs to retrieve wind speed. It is very interesting to compare wind speed estimated by the EM models, general descriptions of radar scattering from sea surface, to the one estimated by the EP models, specific descriptions for the inverse problem. Based on the comparisons, some ideas are proposed to improve the performance of the EM models for wind speed retrieval.

Keywords

C-Band Synthetic Aperture Radar (SAR), Electromagnetic (EM) Scattering Models, Radar Cross-Section (RCS), Remote Sensing, Small Perturbation Model (SPM), Sea Surface Wind

1. Introduction

The exploitations of Synthetic Aperture Radar (SAR) images to retrieve oceanic parameters have been widely studied in the literature, due to many advantages of SAR systems: stable operations in most meteorological con-

How to cite this paper: La, T.V., Khenchaf, A., Comblet, F., Nahum, C. and Ghanmi, H. (2016) Exploitation of Electromagnetic Models for Sea Wind Speed Estimation from C-Band Sentinel-1 Images. *Journal of Electromagnetic Analysis and Applications*, 8, 42-55. <http://dx.doi.org/10.4236/jemaa.2016.83005>

ditions, revisit period, high resolution. Among the important oceanic parameters, sea surface wind plays a crucial role for the studies of the other parameters, *i.e.* waves, currents, marine meteorology, and the coupling of oceanic and atmospheric systems. As well as, surface wind speed is an important parameter in the studies of many oceanic applications, *i.e.* oil slick observation [1], and ship detection [2]. The retrieval of wind fields has been carried out from different SAR data via different approaches [3]-[8]. In such studies, the resolutions of the estimated wind vectors are significantly dependent on the signal-to-noise ratio (SNR) of each SAR system. In practice, one can obtain a $1 \text{ km} \times 1 \text{ km}$ wind cell in cases where the speckle noise level is quite low. In spite of the diverse approaches, the retrieval of wind vectors by using the physical models is particularly preferred, due to their generality. For this approach, one can find two principal methods: via empirical (EP) models, and electromagnetic (EM) models.

The common point of both EP and EM models is the use of the geophysical model functions (GMFs) to describe the dependency of normalized radar cross section (NRCS) on wind speed and the geometry of observations. Therefore, by knowing NRCS and geometric parameters, it is possible to invert the GMFs to estimate wind speed. For the EP models (also known as scatterometry-based approaches), the GMFs are constructed and validated by the series of satellite scatterometer missions. For instance, the C-band GMFs, known as CMOD.4 [9], CMOD.IFR2 [10], CMOD.5 [11], CMOD.5N [12], were derived by using the data from scatterometers onboard the European Remote Sensing 1 and 2 satellites (ERS-1 and ERS-2). The CMOD.5 and CMOD.5N are more widely used than the others, since they can offer good wind speed estimation for most wind regimes. The common point of the EP GMFs is that they are defined for VV-polarization (VV-pol). Thus, a polarization ratio (PR) [13]-[19] should be used when the SAR image is in HH-polarization (HH-pol). In contrast to the EP models, the EM ones are constructed and validated by the physical calculations for the reflections and diffractions between radar scattering and sea surface. Depending on different approaches, we can find a variety of EM models based on the exact methods, *i.e.* Method of Moment (MoM) [20], Forward-Backward Method (FBM) [21], or the asymptotic methods, *i.e.* Small Slope Approximation (SSA) [22], Two-Scale Model (TSM) [23], Small Perturbation Method (SPM) [23]. The advantages and limits of these models have been analyzed and discussed in many references [20]-[23]. In fact, the TSM, SSA, MoM and FBM models can describe radar backscattering from sea surface with different scales of ocean waves, *i.e.* long-, intermediate-, and short-scale waves. Their descriptions are generally complicated due to a lot of variables, relations, and conditions. Meanwhile, for the SPM the description of the relation between radar backscattering and sea surface is quite simpler, since it concerns principally short-scale waves. Under the point of view of the inverse problem, the SPM seems to be more appropriate than the other EM models to estimate wind speed, due to its flexibility of inversion. This is also the initial objective of this study.

In both EM and EP models, wind direction is a crucial parameter for wind speed estimation. It can be obtained from different available wind sources, *i.e.* *in situ* measurements, numeric weather models, retrieval from SAR data, etc. The last approach is the most widely used in the literature, since it can give (almost) immediately the information of wind directions with high resolution. The methods to retrieve wind directions can be divided into two categories: one is in the spectral domain, and the other is in the spatial domain. The most well-known method in the spectral domain is the Fourier Fast Transform (FFT) [24], while the Local Gradient (LG) [25] is the most widely used one in the spatial domain. Generally, wind directions retrieved by the LG have (much) higher resolution than the ones given by the FFT. In fact, the LG can offer a wind cell of $3 \text{ km} \times 3 \text{ km}$, even $1 \text{ km} \times 1 \text{ km}$ in some conditions [25], instead of a cell of $20 \text{ km} \times 20 \text{ km}$ given by the FFT. The common issue of both the LG and FFT is the 180° directional ambiguity of the retrieved wind directions. It can be removed only if wind shadow is present and visible enough in the lee of coastlines, or if there are additional wind source data, *i.e.* *in situ* measurements, SCAT wind data, etc.

The outline of this paper is as follows. In Section 2, the descriptions of the SPM and CMOD.5 are presented in detail. It also includes the analyses of validity domain, and the impact of different variables on the relation between radar backscattering and sea surface. Section 3 presents the data used for the studied models to retrieve wind speed. Section 4 mentions the retrieval of wind directions from SAR images. Section 5 presents the estimation of wind speed by using the SPM and CMOD.5. The obtained results are compared to *in situ* measurements to evaluate. Section 6 discusses the advantages and limits of the SPM for wind speed estimation. Section 7 summarizes the main points of this paper, and proposes the perspectives to improve the performance of the EM models for wind speed retrieval.

2. Methodology

2.1. Small Perturbation Method (SPM)

The SPM, also known as Bragg resonance, was first identified as an important mechanism of radar backscattering from the water surface a long time ago. It was then developed for radar backscattering from the short-scale waves in the ocean by Wright (1966, 1968) [26], Valenzuela (1978) [27], and Plant (1990) [28]. Depending on different approaches, the descriptions of the SPM in terms of equation, parameters, and validity domain are diverse. In this paper, for the monostatic case of radar scattering, we use the definition presented in [23] as shown by (1).

$$\sigma_{pp}^s = 8 \left| k^2 \sigma \cos^2 \theta \alpha_{pp} \right|^2 W(k_x + k \sin \theta, k_y) \quad (1)$$

where σ_{pp}^s denotes the radar backscattering (or NRCS) from sea surface in VV- or HH-pol; k is the radar wave number; k_x, k_y are the x - and y -axis components of k , respectively; θ indicates the radar incident angle (and also backscattering angle in monostatic case); α_{pp} denotes the Bragg coefficients in VV- or HH-pol; σ and W represent the standard deviation and normalized roughness spectrum of sea surface waves, respectively.

The Bragg coefficients in VV- and HH-pol, α_{VV} and α_{HH} , are described as a function of sea water permittivity ϵ_r and incident angle θ , as given by (2) and (3).

$$\alpha_{VV} = \frac{(\epsilon_r - 1) \left[\epsilon_r (1 + \sin^2 \theta) - \sin^2 \theta \right]}{\left[\epsilon_r \cos \theta + \sqrt{(\epsilon_r - \sin^2 \theta)} \right]^2} \quad (2)$$

$$\alpha_{HH} = \frac{\epsilon_r - 1}{\left[\cos \theta + \sqrt{(\epsilon_r - \sin^2 \theta)} \right]^2} \quad (3)$$

The calculations of sea water permittivity have been shown in many references [29]-[32]. The most widely used model is probably the study of Debye [31], and then the double-Debye model [32]. In practice, the significant difference of these models is only noted at very high frequencies. In C-band ($f = 5.4$ GHz), the sea water permittivity calculated by the two Debye models is quite similar [32]. In this paper, for the simple calculations we use the Debye model to calculate ϵ_r , as given by (4).

$$\epsilon_r = \epsilon_\infty(T, S) + \frac{\epsilon_s(T, S) - \epsilon_\infty(T, S)}{1 + j2\pi\nu\tau(T, S)} - j \frac{\sigma}{2\pi\nu\epsilon_0} \quad (4)$$

where $\epsilon_s(T, S)$ and $\epsilon_\infty(T, S)$ are the static and high-frequency dielectric constants, respectively; τ is the relaxation time; ϵ_0 is the permittivity of free space ($\epsilon_0 = 8.854 \times 10^{-12}$ F/m); σ is the ionic conductivity. The temperature T and salinity S of the sea water of the Iroise Coast (France) are collected via www.previmier.org, from Oct. 2014 to Apr. 2015. The temperature T varies between 4°C (Feb. 2015) and 18°C (Oct. 2014), while S is quite stable around 32 - 35 ppt. By using (4), we note that the permittivity of sea water varies slightly from $\epsilon_r = 62.54 + j39.82$ (Feb 2015) to $\epsilon_r = 66.81 + j34.93$ (Oct 2014). It signifies that temperature and salinity do not have significant effects on the calculation of radar backscattering as in (1).

In contrast to temperature and salinity, the roughness spectrum of sea surface is an important parameter for the NRCS calculations. In fact, it concerns a lot of parameters, particularly wind vector which is the favorite one in this paper. For a simple description, σ and W in (1) are replaced by the directional surface wave spectrum $S(K, \Phi)$, with wave propagation referenced to wind direction. The spectrum $S(K, \Phi)$ is generally described by the two parts as given by (5).

$$S(K, \Phi) = S(K, 0) \times f(K, \Phi) \quad (5)$$

where $S(K, 0)$ is the omnidirectional spectrum, and $f(K, \Phi)$ is the angular spreading function. In general, $S(K, 0)$ is influenced by wind speed, while both wind speed and wind direction affect in the description of $f(K, \Phi)$. By knowing $S(K, \Phi)$ and Φ , it is possible to estimate wind speed. One should note that K in (5) is the wavenumber of ocean waves. For the SPM (or Bragg resonance), K relates to the radar wavenumber k in (1) as $K = 2k \times \sin \theta$, where θ is always the radar incident angle.

The theoretical modelling of sea surface roughness spectrum has a history as long as the investigation of radar backscattering from the ocean surface. The initial studies were proposed by Cox and Munk (1954) [33], Pierson and Moskowitz (1964) [34]. It was then developed by Bjerkass and Riedel (1979) [35], Donelan and Pierson (1987) [36], and Apel's (1994) [37]. Based on the previous studies, Elfouhaily *et al.* (1997) [38] were proposed a unified form of sea surface spectrum. This is one of the most widely used models in the literature because it concerns both long- and short-scale waves of the ocean. Then, Kudryavtsev *et al.* (2003) [39] were proposed a new model of sea short-scale wave spectrum. It is preferred in some references, especially for the studies of rain effects on radar backscattering [40]; since it was developed from a balance of wind input, parasitic wave generation, and wave dissipation, and therefore is convenient to modify to include rain effects. However, this model does not work well for wind speed below 5 m/s [39]. Recently, for the reason of rapid and simple calculations of radar backscattering, Hwang *et al.* [41]-[43] have developed an empirical form of sea surface spectrum. This study is based on the conclusion about the dependency of curvature wave spectrum on wind friction velocity and wave phase speed. From the analysis of the studies of sea surface spectrum, we select the Elfouhaily model due to its generality. The comparison of different sea spectrum models will be discussed in the other papers.

The validity condition of the SPM has been discussed in [23] [44], but it seems to be difficult to give the obvious conclusions in terms of wind speed and incident angle, since this condition concerns the mean square slope (mss) of sea wave spectrum used in the SPM. Generally, as indicated in [44] the SPM works well for the root mean square slope ($rmss$) < 0.3 , or mean square slope (mss) < 0.09 . The relation of mss and wind speed has been studied and validated in many studies as discussed in [38]. Among them, the most successful measurements were proposed by Cox and Munk (1954) [33]. For a clean sea surface, the mss is defined as in (6).

$$mss_{clean} = 10^{-3} (3 + 5.12U_{10}) \pm 0.004 \quad (6)$$

where U_{10} is the wind speed at the 10 m height. Equation (6) is only validated under the wind condition: 1 m/s $< U_{10} < 13$ m/s. By combining (6), the conditions of $mss < 0.09$, and 1 m/s $< U_{10} < 13$ m/s, we realize that the validity domain of SPM limits for wind speed below 13 m/s. According to the Beaufort scale, for this level of wind speed, there are only wavelets, sometimes short-scale waves on the sea surface. It signifies that the SPM should be used under the condition of slightly rough sea surface, without the presence of intermediate- or/and long-scale waves. In comparison to the other EM models, which can describe sea surface roughness more generally (*i.e.* TSM, SSA), the SPM works well for moderate incident angles from 32.5° to 45°.

2.2. Comparison of SPM and CMOD5

A general form of the GMFs described in the EP models is defined as in (7) [9]-[12].

$$\sigma_{VV}^0 = A [1 + b_1 \times \cos \Phi + b_2 \times \cos 2\Phi]^B \quad (7)$$

where Φ is the wind direction relative to the radar look direction, A , B , b_1 , b_2 are the functions of U_{10} and θ . Thus, by determining σ_{VV}^0 and θ from the SAR data, and Φ , wind speed U_{10} can be estimated by inverting (7). As indicated, we select the CMOD.5 for the estimation of wind speed, since it can work well for most wind regimes. As well as the SPM, the validity domain of the CMOD.5 is limited under some conditions. The CMOD.5 can work well for the incident angles of 20° - 50°, and for wind speed below 25 - 30 m/s [11]. One should know that the range of 20° - 50° is widely used to acquire images for most SAR systems, and wind speed is rarely beyond 25 - 30 m/s. This signifies that the CMOD.5 is generally a good empirical model to estimate wind speed from SAR data.

Since the EP GMFs are only defined for VV-pol, a polarization ratio, PR , should be used for the SAR images in HH-pol. The calculations of PR have been studied in many references [13]-[18]. They can be divided into two approaches: Thompson model [13], and Mouche model [16]. In the Thompson model, the PR is defined as a function of radar incident angle, as given by (8).

$$PR = \frac{(1 + 2 \tan^2 \theta)^2}{(1 + \alpha \tan^2 \theta)^2} \quad (8)$$

where α is an adjustable parameter. It is calibrated via the *in situ* measurements. In fact, one can find some values of α : $\alpha = 0.6$ in [13], $\alpha = 1.0$ in [14], and $\alpha = 1.2$ in [15]. Contrary to the Thompson model, in [16], Mouche

et al. concluded that the *PR* depends not only on radar incident angle, but also on wind direction. Hence, they proposed a new model for *PR* calculation as given by (9).

$$PR = A_{\phi} \exp(B_{\phi}) + C_{\phi} \quad (9)$$

where A_{ϕ} , B_{ϕ} , and C_{ϕ} are the parameters determined by the *in situ* measurements and SAR images, with regard to the impact of wind directions. Based on the study of Mouche, some studies [17] [18] have re-calculated A_{ϕ} , B_{ϕ} , and C_{ϕ} to better agree with the different C-band SAR data and *in situ* measurements. In this paper, we use the model proposed by Liu *et al.* [18] for wind speed retrieval in HH-pol.

Figure 1 presents the comparison of the NRCS calculated by the SPM with the Elfouhaily wave model (SPM-Elf) and CMOD.5 in VV-pol and HH-pol. The studied values of wind speed and incident angle limit at $u_{10} = 13$ m/s and $\theta = 30^\circ - 45^\circ$ which correspond to the validity domain of the SPM. At $\theta = 30^\circ$, for both up-wind (**Figure 1(a)**) and cross-wind directions (**Figure 1(b)**), the NRCS in VV-pol calculated by the SPM-Elf is (about) 2 - 4 dB lower than that offered by the CMOD.5. At $\theta = 45^\circ$, the two models give quite similar NRCS level for up-wind direction. Meanwhile, for cross-wind direction the level calculated by the SPM-Elf is (about) 2 - 3 dB higher than that of the CMOD.5. In HH-pol, in most cases of incident angle and wind direction, the SPM-Elf underestimates NRCS level in respect with wind speed (about 5 - 7 dB).

The results obtained in **Figure 1** show that in VV-pol, the SPM-Elf can offer similar wind speed estimation to the CMOD.5 for up-wind direction, and a little more for cross-wind direction. This conclusion is noted for moderate incident angles ($32.5^\circ - 45^\circ$). On the contrary, in HH-pol for most cases of incident angle and wind direction, wind speed obtained by the SPM-Elf is overestimated in comparison to the one given by the CMOD.5. This is particularly noted for quite low incident angles ($30^\circ - 32.5^\circ$).

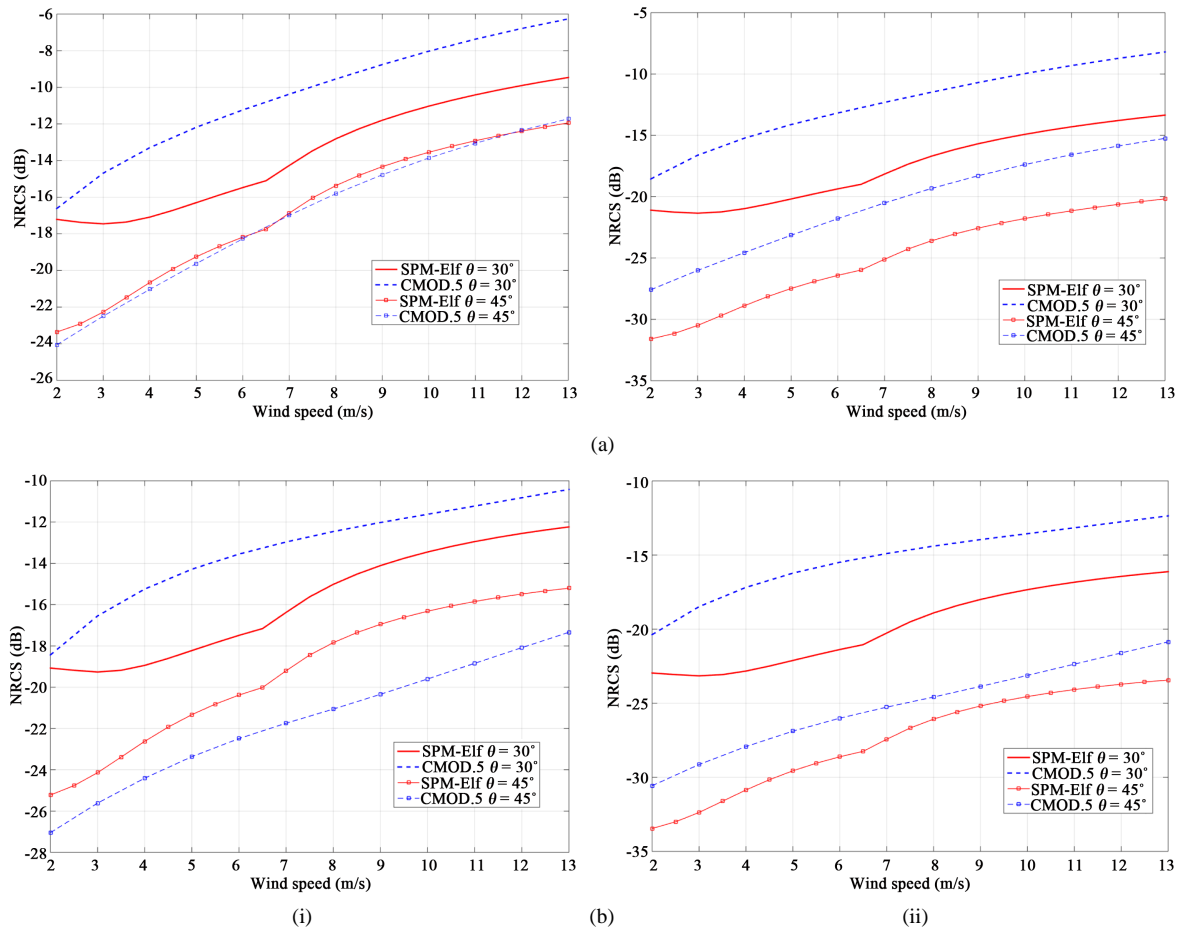


Figure 1. Comparisons of NRCS calculated by SPM with Elfouhaily spectrum (SPM-Elf) and CMOD.5 for $\theta = 30^\circ$ and $\theta = 45^\circ$. (i) VV-pol. (ii) HH-pol. (a) Up-wind direction. (b) Cross-wind direction.

3. Data Preparation

3.1. Sentinel-1 Images

SAR images studied in this paper are acquired by the C-band Sentinel-1 satellite. It was launched in April 2014 by the European Space Agency (ESA), with the aim of providing an independent operational capability for continuous radar mapping of the Earth. The acquisition modes of the Sentinel-1 include: Stripmap (SM), Interferometric Wide Swath (IWS), Extra Wide Swath (EWS), and Wave Model (WM). The images can be acquired in single polarization (VV/HH), or in dual-polarization (VV+VH / HH+HV). In this study, we use the Level-1 images acquired with SM mode in HH-pol, and with IWS mode in VV-pol. They are downloaded via <https://scihub.esa.int>. The acquired data are the type of GRD (Ground Range, Multi-Look, Detected), with high resolution (HR). This type allows reducing speckle noise, but it also decreases the spatial resolution of the image. For instance, the spatial resolution of the studied image in SM mode is reduced to $23 \text{ m} \times 23 \text{ m}$, instead of $3.6 \text{ m} \times 4.9 \text{ m}$. As well, the image in IWS mode has a spatial resolution of $20 \text{ m} \times 22 \text{ m}$, instead of $3.5 \text{ m} \times 22 \text{ m}$.

3.2. In Situ Measurements

The *in situ* measurements used in this paper are collected at the meteorological stations of Météo France along the Iroise Coast (Figure 2), since there are not any fixed meteorological buoys in this area. These stations (red points) are located very close to the open sea. This allows reducing as possible the difference between the measured data along the coast and on the open sea. Since wind speed is measured at different heights, it needs to be corrected to the reference level of 10 m height for comparisons with estimated results. The correction methods of wind speed can be found in [45] [46]. However, the obtained results with the studied models are not much different. In this study, we use a simple power-law varying wind profile as given by (10) [45].

$$\frac{u_2}{u_1} = \left(\frac{z_2}{z_1} \right)^{0.1} \quad (10)$$

where u_2 stands for the wind speed at height z_2 and u_1 and z_1 are the known wind speed and height, respectively.

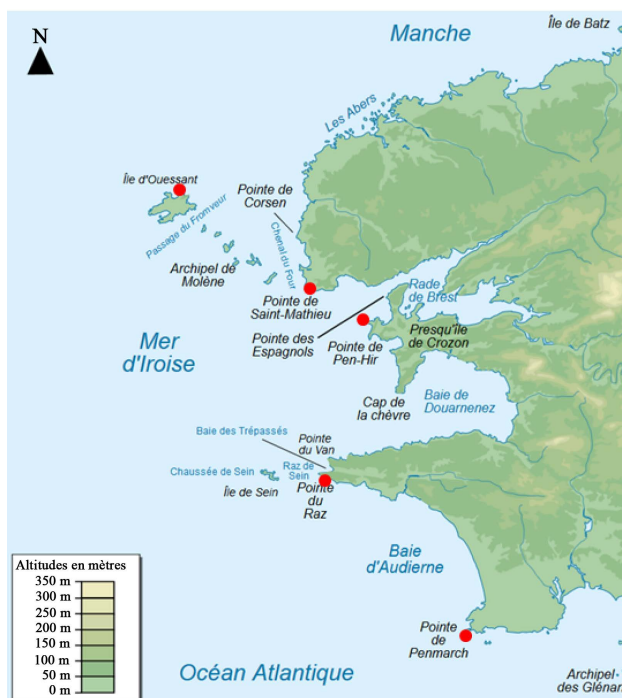


Figure 2. Meteorological stations (red points) of Météo France along the Iroise Coast (France).

4. Wind Direction Extraction

For both SPM and CMOD.5, wind direction is a crucial parameter for wind speed estimation, in particular for high wind speed. However, its impact is not the same for the two models. In fact, for the SPM the effect of wind direction is noted in the angular spreading function of sea roughness spectrum (as in (5)), while it is represented by the $\cos\Phi$ and $\cos2\Phi$ parameters in the CMOD.5 (as in (7)). As shown in **Figure 1**, the NRCS for up-wind direction is higher than the one in cross-wind direction, and this result is noted for both polarizations. Meanwhile, as shown in **Figure 3**, the difference of NRCS in respect to wind direction calculated by the CMOD.5 is more significant than the one calculated by the SPM, in particular between up- and cross-wind directions, and for high wind speed.

The wind direction data can be obtained via many ways, *i.e.* from: a) *in situ* measurements, b) numeric weather models, or c) extraction from SAR images. Among them, the retrieval of wind directions from SAR data is the most widely used, since it can give high wind resolution. In addition, it can be one of the rare choices to have wind direction information in the areas where the fixed meteorological buoys are not installed. As indicated, the LG method is preferred to the FFT one since it can give wind directions with smaller resolution cells (even $1 \text{ km} \times 1 \text{ km}$ in some cases [25]). Since the fundamentals of the LG method have been discussed in many references [25] [47], we only summarize here the main steps and present some important remarks to obtain good extractions.

- 1) First, the filtered images should be reduced dimension sizes to enhance wind streaks, and divided into the sub-images according to expected spatial resolution.
- 2) Then, for each defined sub-image, the histogram of LG directions must be weighted and smoothed.
- 3) After that, the main LG direction of each sub-image is estimated, and the orthogonal of the most frequent gradient direction is assigned as the most available wind direction.
- 4) Finally, the 180° ambiguity of wind direction can be solved either by *in situ* measurements, or via the Continuous Wavelet Transform (CWT) method.

The first step is a crucial task to obtain good extractions in respect to spatial resolution. The spatial resolution of extracted wind directions depends on the acquisition model of SAR images. It can be $1 \text{ km} \times 1 \text{ km}$ if the quality of SAR image is good enough. For the images used in this paper (SM and IWS modes), a wind direction cell of $3 \text{ km} \times 3 \text{ km}$ seems to be enough for the SPM and CMOD.5 to have good spatial resolution of wind speed. The importance of the second step can be verified in **Figure 4**. Due to being weighted and smoothed, the extracted wind directions are very close to the measured data (red arrows). As shown in the right, the difference between the not-smoothed wind direction and measured data is up to 35° , while it is reduced to 5° for the smoothed wind direction.

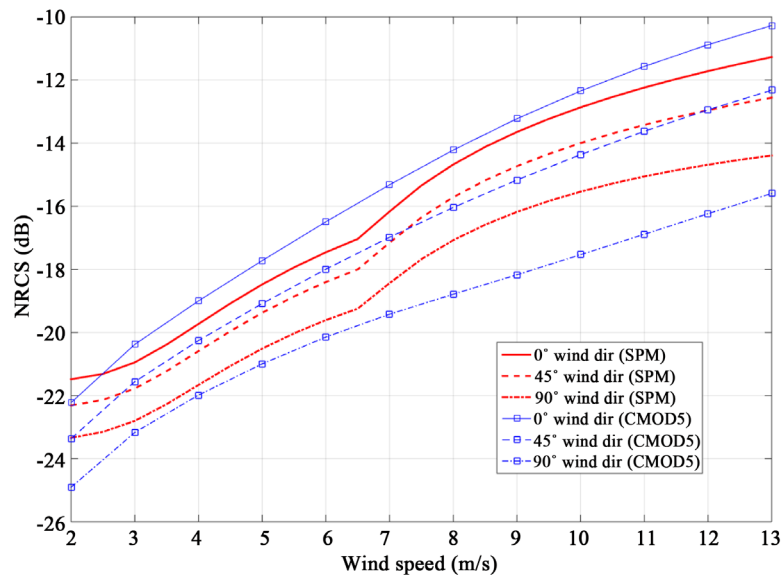


Figure 3. NRCS in respect to wind direction and wind speed studied by the SPM and CMOD.5.

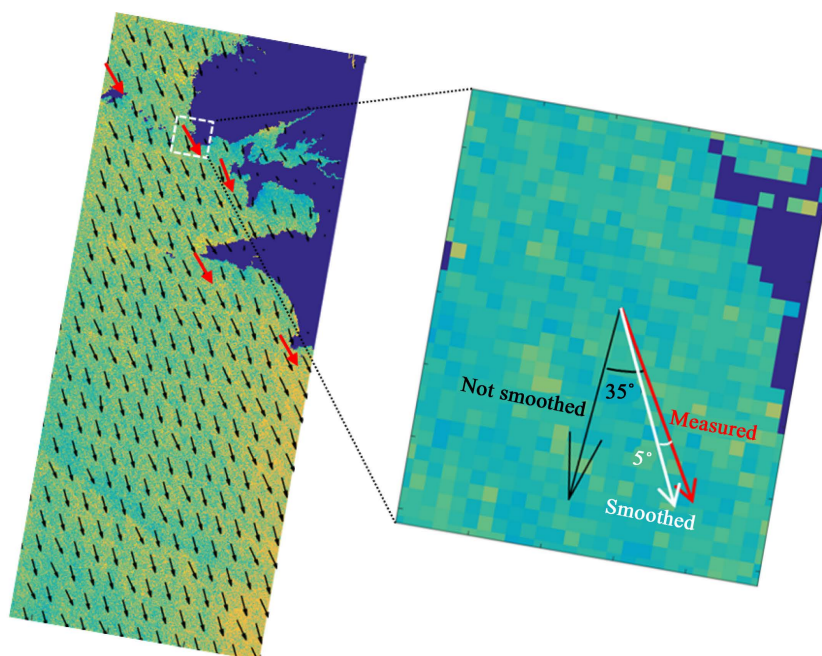


Figure 4. Extraction of wind direction by LG method on a Sentinel-1 image (SM mode), acquired on 27th Dec. 2014 from 06:23:46 UTC to 06:24:15 UTC. (Left) Smoothed vs. measured (red arrows) wind directions. (Right) Main LG direction of a sub-image before and after smoothing, compared to measured wind direction.

One of the most important constraints of the LG method is the 180° ambiguity of the extracted wind directions. It can be solved by *in situ* measurements or numerical weather models. However, the measured data are not always available for all cases. Recently, the CWT method has been developed to solve this problem. Nevertheless, it seems to be complicated to apply. There is another way to solve the 180° ambiguity of extracted wind direction, if wind streaks on SAR images are visible enough to observe. As shown in **Figure 5**, after reducing the dimension sizes of the SAR image presented in **Figure 4**, the wind streaks are much more visible to be noted. Based on this observation, the 180° ambiguity of extracted wind directions can be easily solved. The efficiency of this method depends on the visibility of wind streaks which depends on wind regimes and speckle noise level. For low wind regimes (below 5 m/s), it is generally difficult to determine wind streaks. This is the same in the case where speckle noise is significant.

5. Wind Speed Estimation

Figure 6 describes the indispensable steps to retrieve wind speed from SAR images. The Level-1 Sentinel-1 images are processed by the toolbox for data calibration, land masking, and sub-image division. Thanks to this step, the NRCS of the image is determined. Then, by using the LG method described above, wind directions with different spatial resolutions can be determined. They are compared to the measured data to verify. Finally, the NRCS and wind directions extracted from SAR images are applied in the SPM and CMOD.5 to retrieve wind speed with different spatial resolutions. To evaluate, the estimated wind speed will be compared to the measured data collected at the stations in **Figure 2**.

5.1. VV-Pol Image

Wind speed estimation on a VV-pol Sentinel-1 image by using the SPM and CMOD.5 is presented in **Figure 7**. This image is acquired in IWS mode with radar incident angles from 32.5° to 45° . The spatial resolution of wind direction and wind speed in this case is $3 \text{ km} \times 3 \text{ km}$. As discussed in Section 4, for this level of spatial resolution, the different wind speed areas may be well visualized. As expected from **Figure 1**, for the range of $\theta = 32.5^\circ - 35^\circ$, the wind speed estimated by the SPM is 2 - 3 m/s higher than that given by the CMOD.5. This is al-

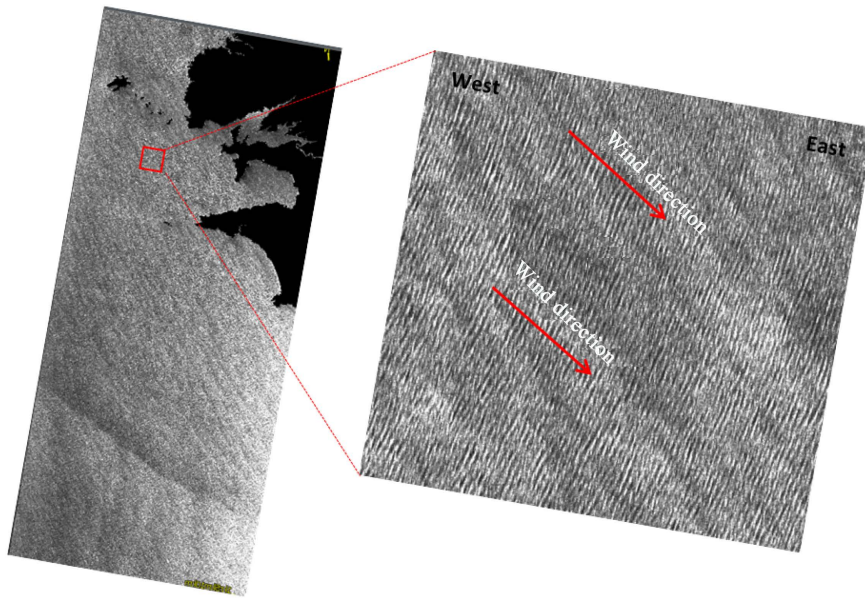


Figure 5. Enhancement of wind streaks on the SAR image presented in **Figure 4** to obtain exact wind direction.

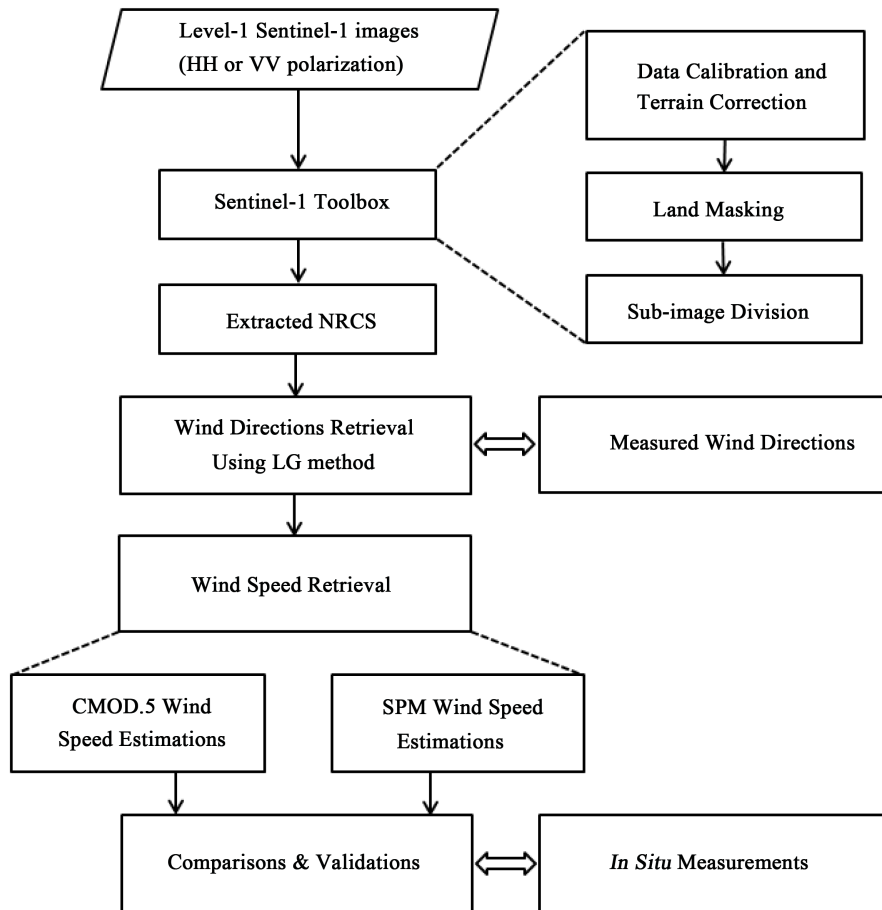
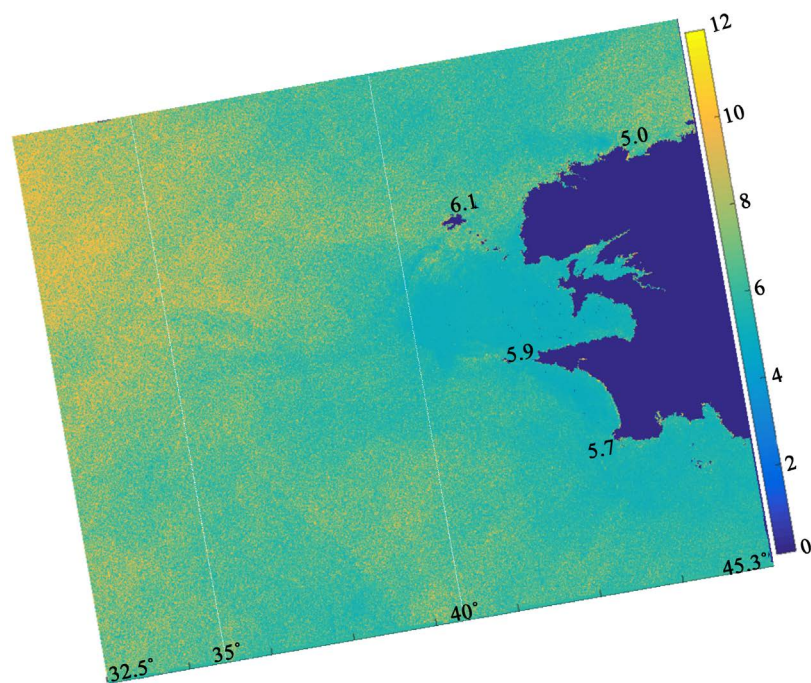
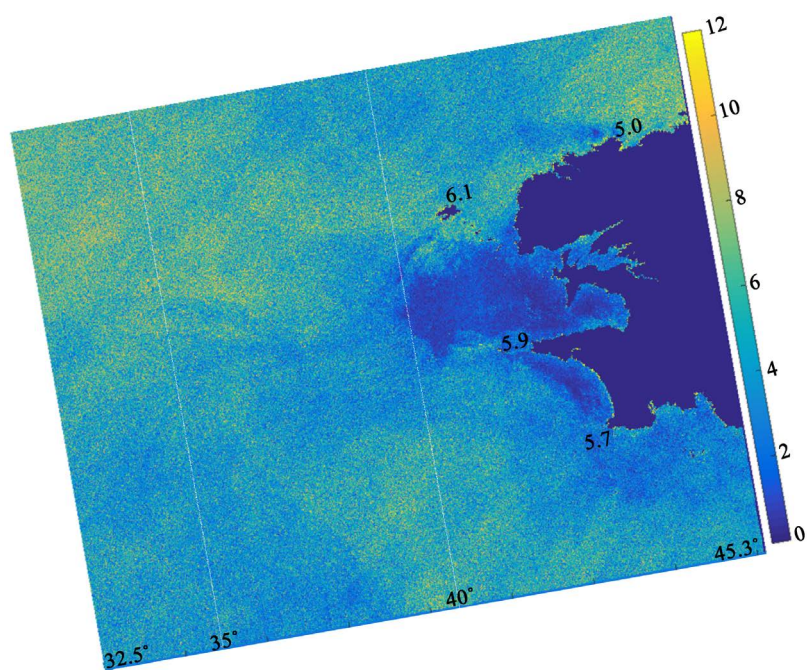


Figure 6. Diagram of wind speed retrieval carried out by the SPM and CMOD.5, from Level-1 Sentinel-1 images in VV- and HH-pol.



(a)



(b)

Figure 7. Map of wind speed estimated by the SPM (a) and CMOD.5 (b) from a VV-pol Sentinel-1 image in IWS mode acquired on 15th Apr 2015, from 18:12:46 UTC to 18:13:15 UTC.

so noted for $\theta = 35^\circ - 40^\circ$, but the deviation is less significant (only about 1 - 2 m/s). For $\theta = 40^\circ - 45^\circ$, the SPM and CMOD.5 give (quite) similar wind speed estimation. They are also very close to the measured data (the same range of 5 - 7 m/s). Compared to the SPM, the CMOD.5 seems to give higher spatial resolution of wind speed, especially for the range of 1 - 5 m/s. Indeed, the noted minimum value of the SPM wind speed is about 4 - 5 m/s, while it is 0 - 1 m/s for the CMOD.5 wind speed.

5.2. HH-Pol Image

Figure 8 shows the wind speed estimations on a HH-pol Sentinel-1 image by using the SPM and CMOD.5. This image is acquired in SM mode with radar incident angles from 42° to 46° . As well as in the previous case, the spatial resolution of wind direction and wind speed in this case is $3 \text{ km} \times 3 \text{ km}$. As expected from **Figure 1**, SPM overestimates wind speed in most cases of incident angle and wind direction. That can be verified in this case. While the wind speed estimated by the CMOD.5 is only in the range of 10 m/s - 15 m/s, that of the SPM is 10 - 15 m/s higher. This is confirmed by the comparisons with the measured data which are only in the range of 10 - 16 m/s. As well as in **Figure 7**, the $3 \text{ km} \times 3 \text{ km}$ spatial resolution gives the good distinction of wind speed areas. In particular, in contrast to the previous case, the wind streaks can be well noted in this case. This is an important sign to solve the 180° ambiguity of extracted wind direction, as discussed in **Figure 4** and **Figure 5**.

6. Discussion and Validation

For the Sentinel-1 data in VV-pol, wind speed estimated by the SPM is quite similar to the one offered by the CMOD.5 for the range of $\theta = 32.5^\circ$ to 45° . The deviation of 2 - 3 m/s is tolerable in some applications (e.g. weather forecasting). Certainly, this conclusion is only validated in the wind speed range of 1 - 12 m/s, corresponding to the validity domain of the SPM. Nevertheless, from our study, the SPM still gives (quite) similar wind speed estimation to the CMOD.5 for wind speed above 12 m/s. This result is only acceptable under the point of view of mathematics. It has not any physical significance. However, if the SPM is corrected to widen the validity domain of wind speed and incident angle, it can be used to estimate wind speed from SAR images as the EP models. Indeed, the TSM is a good successive model of the SPM to study radar backscattering with higher wind speed and different ranges of incident angles [23]. In **Figure 7**, the wind speed estimated by the SPM has lower spatial resolution than that of the CMOD.5. This is probably from the sea surface roughness spectrum studied in this paper, or from the SPM. Therefore, to well understand, the other wave spectrum models should be taken into account in the next paper.

For the images in HH-pol, the SPM overestimates wind speed in most cases of incident angle and wind direction. This result can be explained by some facts. First, the polarizations of radar backscattering respond to sea

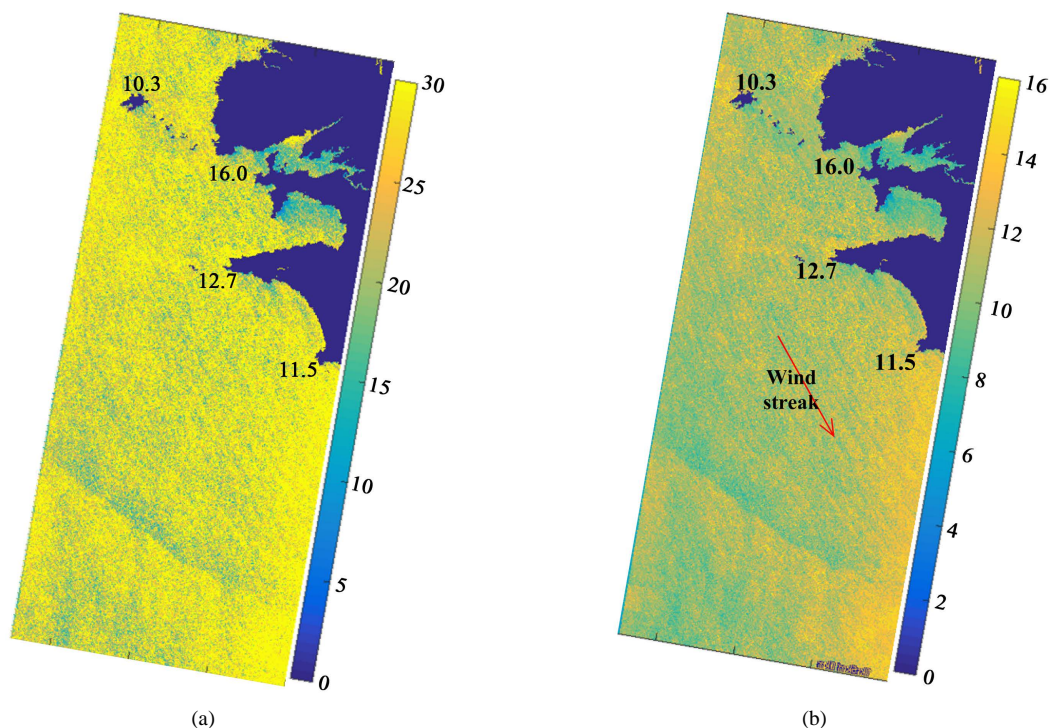


Figure 8. Map of wind speed estimated by the SPM (a) and CMOD.5 (b) from a HH-pol Sentinel-1 image in SM mode acquired on 27th Dec 2014, from 18:12:46 UTC to 18:13:15 UTC.

surface roughness and wave breaking differently. In fact, as shown in many studies [26]-[28], VV-pol is dominated by Bragg resonance scattering, while non-Bragg scattering mechanisms is more appropriate for HH-pol (maybe VH-pol). In other words, the SPM can describe well radar backscattering in VV-pol, while for HH-pol the other EM models (*i.e.* TSM, SSA) should be used. Second, long wind waves are not aligned with local wind, and there may be waves, *i.e.* swell, not related to the local wind. Furthermore, the sea can be partially developed, and this makes the wave spectrum different from the standard reference ones (*i.e.* Elfouhaily). In other words, while the standard models assume that the roughness statistics are homogenous, in practice, they vary nonlinearly. This constraint for HH-pol is more sensitive than for VV-pol because NRCS in HH-pol is normally several dBs lower than NRCS in VV-pol. Therefore, a non-linear spectral description of sea surface roughness should be used to improve wind speed estimation.

7. Conclusions and Perspectives

This paper has discussed about the application of the EM models to estimate wind speed from SAR data. Under the point of view of the inverse problem, the SPM has been selected due to its flexibility of inversion. Nevertheless, it can only work well for wind speed below 13 m/s, and for moderate incident angles of $32.5^\circ - 45^\circ$. The wind speed estimated by the SPM is specifically compared to the one offered by the CMOD.5. The CMOD.5 is a widely used empirical model in the literature to estimate wind speed from SAR data. In both studied models, wind direction plays an important role to estimate accurately wind speed. In the indicated validity domain (wind speed below 13 m/s and incident angles of $32.5^\circ - 45^\circ$), the SPM gives quite similar wind speed estimation to the CMOD.5 in VV-pol. However, the resolution of wind speed obtained by the SPM is lower than that of the CMOD.5. In HH-pol, the SPM overestimates wind speed in most cases of incident angle and wind direction. This result can be explained by some facts which concern the different behavior of radar backscattering to polarization, and the difference between the standard wave spectrum used in the SPM and the practical one at the moment of SAR image acquisition.

In the next steps, in order to improve the validity domain of the SPM, the other EM models like TSM or SSA should be used. They are expected to possibly estimate wind speed above 13 m/s, and for different ranges of incident angles, notably for $\theta = 20^\circ - 30^\circ$. In particular, to improve wind speed estimation in HH-pol, together with the other EM models, a study of sea surface roughness spectrum should be done.

Acknowledgements

This work is supported by the French General Directorate for Armament (DGA) in the frame of Project SIMUSO. TheSentine-1 images are provided by the European Space Agency (ESA) via <https://scihub.esa.int/>. The *in situ* measurements are collected via <http://www.infoclimat.fr/>.

References

- [1] Ghanmi, H., Khenchaf, A. and Comblet, F. (2014) Numerical Modeling of Electromagnetic Scattering from Sea Surface Covered by Oil. *Journal of Electromagnetic Analysis & Applications*, **6**, 15-24. <http://dx.doi.org/10.4236/jemaa.2014.61003>
- [2] Pino, M.R., Landesa, L., Rodriguez, J.L., Obelleiro, F. and Burkholder, R.J. (1999) The Generalized Forward-Backward Method for Analyzing the Scattering from Targets on Ocean-Like Rough Surfaces. *IEEE Transactions on Antennas and Propagation*, **47**, 961-969.
- [3] Shimada, T., Kawamura, H. and Shimada, M. (2003) An L-Band Geophysical Model Function for SAR Wind Retrieval Using JERS-1 SAR. *IEEE Transactions on Geoscience and Remote Sensing*, **41**, 518-531.
- [4] Lehner, S., Schulz-Stellenfleth, J., Schättler, B., Breit, H. and Horstmann, J. (2000) Wind and Wave Measurements Using Complex ERS-2 SAR Wave Mode Data. *IEEE Transactions on Geoscience and Remote Sensing*, **38**, 2246-2257.
- [5] Carvajal, G.K., Eriksson, L.E.B. and Ulander L.M.H. (2014) Retrieval and Quality Assessment of Wind Velocity Vectors on the Ocean with C-Band SAR. *IEEE Transactions on Geoscience and Remote Sensing*, **52**, 2519-2537.
- [6] Horstmann, J., Koch, W., Lehner, S. and Tonboe, R. (2000) Wind Retrieval over the Ocean Using Synthetic Aperture Radar with C-Band HH Polarization. *IEEE Transactions on Geoscience and Remote Sensing*, **38**, 2122-2131.
- [7] Li, X.-M. and Lehner, S. (2014) Algorithm for Sea Surface Wind Retrieval From TerraSAR-X and TanDEM-X Data. *IEEE Transactions on Geoscience and Remote Sensing*, **52**, 2928-2939.

- [8] Montuori, A., de Ruggiero, P., Migliaccio, M., Pierini, S. and Spezie, G. (2013) X-Band COSMO-SkyMed wind Field Retrieval, with Application to Coastal Circulation Modeling. *Ocean Science*, **9**, 121-132. <http://dx.doi.org/10.5194/os-9-121-2013>
- [9] Stoffelen, A. and Anderson, D. (1997) Scatterometer Data Interpretation: Estimation and Validation of the Transfer Function CMOD4. *Journal of Geophysical Research*, **102**, 5767-5780. <http://dx.doi.org/10.1029/96JC02860>
- [10] Quilfen, Y., Chapron, B., Elfouhaily, T., Katsaros, K. and Tournadre, J. (1998) Observation of Tropical Cyclones by High-Resolutions Scatterometry. *Journal of Geophysical Research*, **103**, 7767-7786. <http://dx.doi.org/10.1029/97JC01911>
- [11] Hersbach, H., Stoffelen, A. and de Haan, S. (2007) An Improved C-Band Scatterometer Ocean Geophysical Model Function: CMOD5. *Journal of Geophysical Research*, **112**, C03006. <http://dx.doi.org/10.1029/2006JC003743>
- [12] Verspeek, J., Stoffelen, A., Portabella, M., Bonekamp, H., Anderson, C. and Saldaña, J.F. (2010) Validation and Calibration of ASCAT Using CMOD5.n. *IEEE Transactions on Geoscience and Remote Sensing*, **48**, 386-395.
- [13] Thompson, D.R., Elfouhaily, T.M. and Chapron, B. (1998) Polarization Ratio for Microwave Backscattering from the Ocean Surface at Low to Moderate Incidence Angles. *Geoscience and Remote Sensing Symposium Proceedings (IGARSS'98)*, Seattle, 6-10 July 1998, 1671-1673. <http://dx.doi.org/10.1109/igarss.1998.692411>
- [14] Horstmann, J., Koch, W., Lehner, S. and Tonboe, R. (2002) Ocean Winds from RADARSAT-1 ScanSAR. *Canadian Journal of Remote Sensing*, **28**, 524-533. <http://dx.doi.org/10.5589/m02-043>
- [15] Vachon, P.W. and Dobson, F.W. (2000) Wind Retrieval from RADARSAT SAR Images: Selection of a Suitable C-Band Polarization Wind Retrieval Model. *Canadian Journal of Remote Sensing*, **26**, 306-313. <http://dx.doi.org/10.1080/07038992.2000.10874781>
- [16] Mouche, A.A., Hauser, D. and Kudryavtsev, V. (2006) Radar Scattering of the Ocean Surface and Sea-Roughness Properties: A Combined Analysis from Dual-Polarizations Airborne Radar Observations and Models in C Band. *Journal of Geophysical Research: Oceans*, **111**, C09039. <http://dx.doi.org/10.1029/2005JC003166>
- [17] Zhang, B.A., Perrie, W. and He, Y.J. (2011) Wind Speed Retrieval from RADARSAT-2 Quad-Polarization Images Using a New Polarization Ratio Model. *Journal of Geophysical Research: Oceans*, **116**, C00D11.
- [18] Liu, G., Yang, X., Li, X., Zhang, B., Pichel, W., Li, Z. and Zhou, X. (2013) A Systematic Comparison of the Effect of Polarization Ratio Models on Sea Surface Wind Retrieval from C-Band Synthetic Aperture Radar. *IEEE Journal of Selected Topics in Applied Earth Observations and Remote Sensing*, **6**, 1100-1108.
- [19] Ren, Y., Lehner, S., Brusch, S., Li, X.-M. and He, M. (2012) An Algorithm for the Retrieval of Sea Surface Wind Fields Using X-Band TerraSAR-X Data. *International Journal of Remote Sensing*, **33**, 7310-7336. <http://dx.doi.org/10.1080/01431161.2012.685977>
- [20] Colliander, A. and Ylä-Oijala, P. (2007) Electromagnetic Scattering from Rough Surface Using Single Integral Equation and Adaptive Integral Method. *IEEE Transactions on Antennas and Propagation*, **55**, 3639-3646.
- [21] Holliday, D., DeRaad, L.L. and St-Cyr, G.J. (1996) Forward-Backward: A New Method for Computing Low-Grazing Angle Scattering. *IEEE Transactions on Antennas and Propagation*, **44**, 722-729.
- [22] Awada, A., Ayari, Y., Khenchaf, A. and Coatanhay, A. (2007) Bistatic Scattering from an Anisotropic Sea Surface: Numerical Comparison between the First-Order SSA and the TSM Models. *Waves in Random and Complex Media*, **16**, 383-394. <http://dx.doi.org/10.1080/17455030600844089>
- [23] Khenchaf, A. (2001) Bistatic Scattering and Depolarization by Randomly Rough Surface: Application to Natural Rough Surface in X-Band. *Waves in Random and Complex Media*, **11**, 61-89. <http://dx.doi.org/10.1088/0959-7174/11/2/301>
- [24] Fetterer, F., Gineris, D. and Wackerman, C.C. (1998) Validating a Scatterometer Wind Algorithm for ERS-1 SAR. *IEEE Transactions on Geoscience and Remote Sensing*, **36**, 479-492.
- [25] Koch, W. (2004) Directional Analysis of SAR Images Aiming at Wind Direction. *IEEE Transactions on Geoscience and Remote Sensing*, **42**, 702-710.
- [26] Wright, J.W. (1966) Backscattering from Capillary Waves with Application to Sea Clutter. *IEEE Transactions on Antennas and Propagation*, **14**, 749-754.
- [27] Valenzuela, G.R. (1978) Theories for the Interaction of Electromagnetic and Oceanic Waves—A Review. *Boundary-Layer Meteorology*, **13**, 61-85. <http://dx.doi.org/10.1007/BF00913863>
- [28] Plant, W.J. (1990) Bragg Scattering of Electromagnetic Waves from the Air/Sea Interface. In: Geernaert, G.L. and Plant, W.L., Eds., *Environmental Fluid Mechanics. Vol. 8. Surface Waves and Fluxes*, Kluwer Academic Publishers, Dordrecht, 41-108.
- [29] Klein, L.A. and Swift, C.T. (1977) An Improved Model for the Dielectric Constant of Sea Water at Microwave Frequencies. *IEEE Journal of Oceanic Engineering*, **2**, 104-111. <http://dx.doi.org/10.1109/JOE.1977.1145319>

- [30] Stogryn, A. (1971) Equations for Calculating the Dielectric Constant of Saline Water. *IEEE Transactions on Microwave Theory and Techniques*, **19**, 733-736.
- [31] Guillou, C., Ellison, W., Eymard, L., Lamkaouchi, K., Prigent, C., Delbos, G., Balana, G. and Boukabara, S.A. (1998) Impact of New Permittivity Measurements on Sea Surface Emissivity Modeling in Microwaves. *Radio Science*, **33**, 649-667. <http://dx.doi.org/10.1029/97RS02744>
- [32] Meissner, T. and Wentz, F.J. (2004) The Complex Dielectric Constant of Pure and Sea Water from Microwave Satellite Observations. *IEEE Transactions on Geoscience and Remote Sensing*, **42**, 1836-1849. <http://dx.doi.org/10.1109/TGRS.2004.831888>
- [33] Cox, C.S. and Munk, W.H. (1954) Statistics of the Sea Surface Derived from Sun Glitter. *Journal of Marine Research*, **13**, 198-227.
- [34] Pierson, W. and Moskowitz, L. (1964) A Proposed Spectral form for Fully Developed Wind Sea Based on the Similarity Theory of S. A. Kitaigorodskii. *Journal of Geophysical Research*, **69**, 5181-5190. <http://dx.doi.org/10.1029/JZ069i024p05181>
- [35] Bjerkaas, A.W. and Riedel, F.W. (1979) Proposed Model for the Elevation Spectrum of a Wind-Roughened Sea Surface. Technical Report APL-TG-1328-1-31, Applied Physics Laboratory, The Johns Hopkins University, Laurel, 31.
- [36] Donelan, M.A., Hamilton, J. and Hui, W.H. (1985) Directional Spectra of Wind Generated Waves. *Philosophical Transactions of the Royal Society of London. Series A*, **315**, 509-562.
- [37] Apel, J.R. (1994) An Improved Model of the Ocean Surface Wave Vector Spectrum and Its Effects on Radar Backscatter. *Journal of Geophysical Research*, **99**, 16269-16291. <http://dx.doi.org/10.1029/94JC00846>
- [38] Elfouhaily, T.M., Chapron, B., Katsaros, K. and Vandermark, D. (1997) A Unified Directional Wave Spectrum for Long and Short Wind-Driven Waves. *Journal of Geophysical Research: Oceans*, **102**, 15781-15796. <http://dx.doi.org/10.1029/97JC00467>
- [39] Kudryavtsev, V.N., Hauser, D., Caudal, G. and Chapron, B. (2003) A Semi-Empirical Model of the Normalized Radar Cross-Section of the Sea Surface: 1. Background Model. *Journal of Geophysical Research*, **108**.
- [40] Contreras, R.F. and Plant, W. (2006) Surface Effect of Rain on Microwave Backscatter from the Ocean: Measurements and Modeling. *Journal of Geophysical Research: Oceans*, **111**, C08019.
- [41] Hwang, P. and Wang, D.W. (2004) An Empirical Investigation of Source Term Balance of Small Scale Surface Waves. *Geophysical Research Letters*, **31**, L15301. <http://dx.doi.org/10.1029/2004GL020080>
- [42] Hwang, P. (2008) Observations of Swell Influence on Ocean Surface Roughness. *Journal of Geophysical Research: Oceans*, **113**, C12024. <http://dx.doi.org/10.1029/2008JC005075>
- [43] Hwang, P. (2011) A Note on the Ocean Surface Roughness Spectrum. *Journal of Atmospheric and Oceanic Technology*, **28**, 436-443. <http://dx.doi.org/10.1175/2010JTECHO812.1>
- [44] Ulaby, F.T., Moore, R.K. and Fung, A.K. (1986) Microwave Remote Sensing: Active and Passive. Vol. 2. Radar Remote Sensing and Surface Scattering and Emission Theory. Ch. 12, Artech House Publishers, Norwood, 962-966.
- [45] Smith, S. (1988) Coefficients for Sea Surface Wind Stress, Heat Flux, and Wind Profiles as a Function of Wind Speed and Temperature. *Journal of Geophysical Research: Oceans*, **93**, 15467-15472.
- [46] Hsu, S.A., Meindl, E.A. and Gilhousen, D.B. (1994) Determining the Power-Law Wind-Profile Exponent under Near-Neutral Stability Conditions at Sea. *Journal of Applied Meteorology*, **33**, 757-765. [http://dx.doi.org/10.1175/1520-0450\(1994\)033<0757:DTPLWP>2.0.CO;2](http://dx.doi.org/10.1175/1520-0450(1994)033<0757:DTPLWP>2.0.CO;2)
- [47] Carvajal, G.K., Eriksson, L.E.B. and Ulander, L.M.H. (2014) Retrieval and Quality Assessment of Wind Velocity Vectors on the Ocean with C-Band SAR. *IEEE Transactions on Geoscience and Remote Sensing*, **52**, 479-492.